Pattern diversity antenna for on-body and off-body WBAN links

Sema DUMANLI[*]

Department of Electrical and Electronics Engineering, Faculty of Engineering, Boğaziçi University, İstanbul, Turkey

Abstract: Maintaining the quality and the reliability of a wireless body area network (WBAN) has a variety of challenges, one of which is the design of the on-body antenna. The on-body antenna often forms both on-body and off-body links and needs to have an application-specific pattern to secure the connection. The antenna should direct its energy in parallel to the human skin while establishing an on-body link, ideally omnidirectionally, while an on-body link would benefit from a directional radiation pattern perpendicular to human skin. Moreover, the lossy body tissue is within the reactive region of the antenna affecting the antenna performance; hence, the antenna design flow should include this effect. Here a novel antenna is presented that creates the aforementioned radiation patterns using two switches. For the on-body and the off-body links, the TM_{00} and the TM_{01} modes are excited, respectively. The TM_{00} mode generates a quasi-omnidirectional pattern with a simulated directivity of 2 dB in the horizontal plane while the TM_{01} mode generates a directional pattern with a directivity of 4.5 dB. Both modes are matched at the 2.45 GHz ISM band. Finally, using numerical and physical phantoms and male subjects, the antenna has been shown to perform well near human bodies: insignificant detuning was observed and the degradation in the radiation efficiency was measured to be 17% in the worst-case scenario of locating the antenna on the body with 0 mm separation. Note that the size of the antenna is no bigger than a conventional half-wavelength patch antenna.

Key words: Radiation patterns, patch antennas, body area networks

1. Introduction

A wireless body area network (WBAN) can include in-body sensors, on-body sensors, and off-body gateways. Links between these devices can be categorized into three types: in-body, on-body, and off-body links. The on-body sensor often forms both on-body and off-body links while connecting to another on-body sensor/gateway or an off-body gateway. The optimum radiation pattern changes depending on the link as well as the channel itself due to the mobility of the human body. A comparison of directional and omnidirectional antennas in terms of off-body channel gain was given in [1] while a similar comparison was performed for on-body channel gain in [2]. Radiation pattern diversity can be exploited to tackle both the dynamic conditions and the different requirements of the various links formed.

During the design of an on-body antenna, several parameters should be taken into consideration. In order for an on-body sensor to form reliable communication under any circumstances, the antenna should reconfigure its radiation pattern as discussed earlier. The conventional way for that is to use an array of antennas, which is not suitable for the 2.4 GHz ISM band since space is a critical factor. Finally, locating the antenna near body tissue naturally alters the radiation pattern, decreases the radiation efficiency due to absorption by lossy tissue,

[*]Correspondence: sema.dumanli@boun.edu.tr

and detunes the resonance and the matching [3,4]. Accordingly, the requirements of an on-body antenna can be summarized as follows:

1) Able to reconfigure radiation pattern,

2) Isolated from the human body,

3) Small or flexible,

4) Unobtrusive and thin.

Numerous on-body antennas were proposed in the literature. An overview of fabric patch antennas was given in [5]. A button antenna with dual-band operation was proposed in [6]. A PIFA was examined in the proximity of the human body in [7]. Reference [8] presented a disk-loaded monopole to be used on-body. A comparison analysis was given comparing a monopole, a PIFA, an IFA, a printed loop, and a printed dipole in [9]. From the state of the art, it can be inferred that the performances of the monopole and the PIFA are superior in forming on-body links due to their radiation characteristics. Their maximum radiation direction is along the body surface with vertical polarization matching the surface waves [8,10]. Nevertheless, none of these proposals are agile and they fail to satisfy the first requirement. A multimode wearable antenna was proposed in [11]. It achieved three different radiation patterns, all of which are along the human skin, serving the formation of on-body links only where it fails to generate any off-body pattern vertical to the body surface. The work in [12] creates two modes in a manner similar to [11] with no vertical radiation. A multimode antenna with two radiators creating both on-body and off-body modes was proposed in [4]. Although its performance was immune to nearfield effects, it fails to satisfy the fourth requirement with a three-layered thick profile. Another pattern diversity antenna with a stack-up configuration was proposed in the context of MIMO communications in [13]. To the author's knowledge, an on-body antenna satisfying all the listed requirements has not been proposed prior to [14]. A novel shorted patch antenna that can excite two different modes suitable for both on-body and off-body links was previously described by the author in [14]. The antenna is isolated from the body with a ground plane and has a thin profile. It is also suitable for printing on fabric. Here, this antenna is analyzed further in the context of WBANs through measurements on physical phantoms and on two different male subjects with different body fat indices as well as numerical phantoms.

In Section 2 and Section 3, the proposed antenna and the measurement set-up are detailed. Section 4 explains the antenna performance for both modes. The paper concludes in Section 5.

2. Antenna design

The TM_{00} mode of a shorted rectangular patch antenna creates an omnidirectional radiation pattern. Although the TM_{00} mode of a shorted rectangular patch has not been investigated extensively, it is analogous to the widely studied TM_{01} mode of the shorted ring patch antennas [15–17]. The TMm mode mentioned in [18] also describes the generation of the omnidirectional mode in noncircular patches. Application of it to BANs was discussed in [4] and it was compared with a rectangular patch and a monopole near the body surface. The shorted patch was shown to be superior for on-body links. Here an antenna capable of generating this omnidirectional mode and a directional mode is designed.

A novel on-body antenna is designed to operate at the 2.4 GHz ISM band using the ANSYS Electronics Desktop [19] and prototyped. Its size is smaller than $0.5\lambda \times 0.5\lambda$ and dielectric loading can be used for miniaturization.

As seen in Figure 1, it comprises a square patch with a length of pl and a full square ground plane

underneath with a length of sl. The radiating patch is printed on 0.127-mm RT/duroid5880 with 17-μm-thick copper. The patch and the ground plane are separated with 4.8-mm-thick polyethylene foam by Emerson and Cuming. The ground plane is shorted to the patch at symmetrical shorting pins. The shorting pin positions (sd) and their radii (pr) are optimized and the optimum values are listed in Table 1.
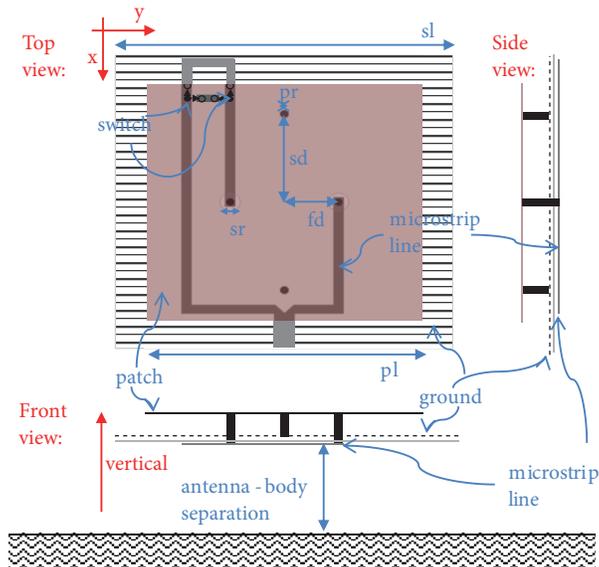

Figure 1. Top, front, and side view of the proposed dual mode antenna, which comprises a switching mechanism to switch between two radiation modes: horizontally omnidirectional and broadside radiation.

Table 1. Antenna design parameters.

| Parameter	pl	sl	fd	sd	pr	sr
Optimized value	45 mm	50 mm	8 mm	15 mm	0.64 mm	0.9 mm

Beneath the ground plane, a feeding network is etched on 1.6-mm-thick FR4 substrate with 35-μm-thick copper. The ground plane of the patch is used as the ground plane of the microstripline feeding network, as well. The network excites the patch at two symmetrical points while these feeding points are isolated from the ground plane with two circular slots. The position of these feed points (fd) and the radii of the slots (sr) are also optimized and the optimum values are listed in Table 1. The feed line comprises a T junction and its branches with unequal length are connected to the aforementioned symmetrical feed points. Being unequal, the length of the branches causes a phase difference, which can be changed by altering the length of one branch by means of a switching mechanism as seen in Figure 1.

The antennas prototyped in-house are shown in Figure 2. Two prototypes with altered branches were manufactured to test both modes. The switches that are supposed to change the length were not included in the design at this stage of the project and are left as future work after validation.

Figure 3 shows the E field in vector form created by each mode: TM_{00} and TM_{01}. As visible in Figure 3a, feeding the excitation points with $0°$ phase difference will activate TM_{00}. Practically, the phase difference can be greater than $0°$ for matching purposes as long as it is less than $90°$. Once it is greater than $90°$, the uniformity of the radiation pattern along φ will be severely distorted. On the other hand, as seen in Figure 3b, having the E field vectors in opposite directions at the excitation points will activate the TM_{01} mode. Hence,
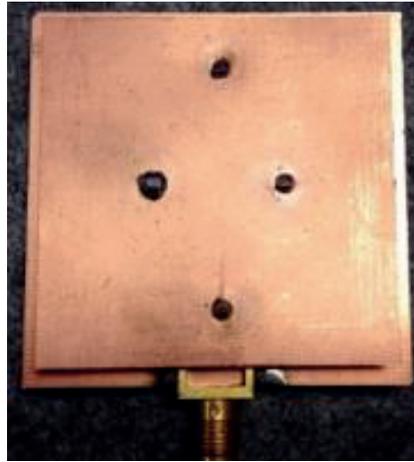
(a) Top view of the prototypes
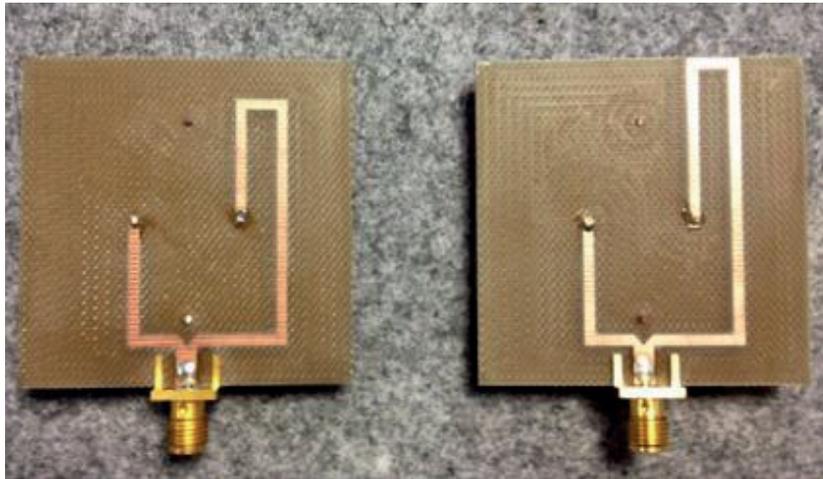
(b) Back view of the on-body mode and the off-body mode antennas respectively

Figure 2. The prototyped on-body and off-body antennas: a) top view of the prototypes; b) back view of the on-body mode and the off-body mode antennas, respectively.

the phase difference should be $180°$. Similarly, this value can be decreased for matching purposes as long as it is more than $90°$, which will generate a more directional radiation suitable for off-body operation. Here the length of the longer branch is decreased by $\lambda/4$ to switch between two modes. Note that the length of the shorter branch is 28 mm and the longer branch is changed from 73 mm to 85 mm.

3. Measurement set-up

The performance of the antennas is tested through simulations and measurements in terms of the frequency response, the gain pattern, and the radiation efficiency. The antennas are evaluated in the following scenarios:

- 18 cm × 18 cm flat chest phantom,
- Male subject, 183 cm tall, 75 kg (Subject A),
- Male subject, 170 cm tall, 64 kg (Subject B),
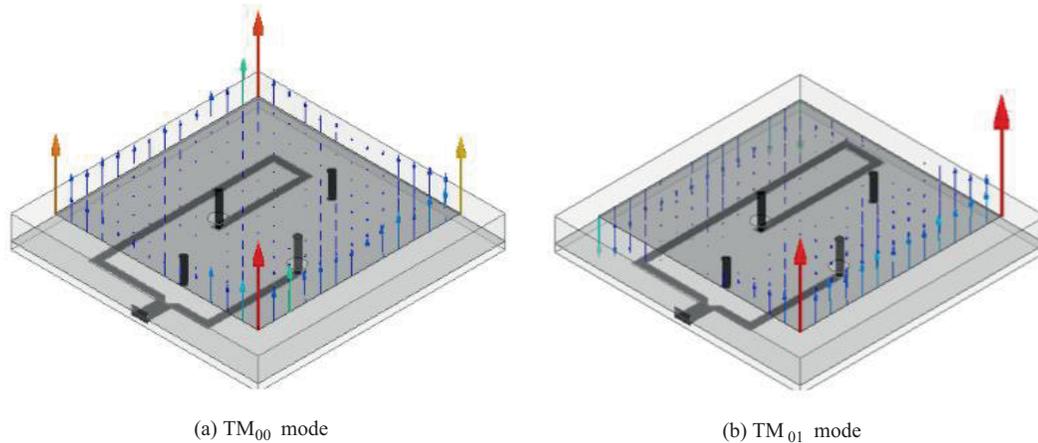- 20 cm × 20 cm radiation-absorbent material (RAM) block.

(a) TM_{00} mode   (b) TM_{01} mode

Figure 3. Vector E field distributions of TM_{00} (a) and TM_{01} (b) modes, which support on-body and off-body operations, respectively.

The frequency response analysis is performed for all these scenarios with different antenna-body separations. However, the radiation characteristics are investigated only on the RAM block and the phantom due to the difficulty in taking 3D radiation pattern measurements of a human being. The radiation pattern of the antennas when located on the chest of a human are approximated by means of a physical chest phantom built at the University of Bristol. The human body is composed of several types of tissues with different frequency-dependent relative permittivity and conductivity values [20]. The permittivity values at 2.45 GHz were calculated to be 52, 37, 42, and 5 for muscle, dry skin, wet skin, and fat, respectively [21]. Therefore, reproducing the average conditions of human flesh, a dielectric constant of 45–50 is sought in the ISM band [22]. An $18 \times 18 \times 2$ cm flat phantom with relative permittivity of 45 and conductivity of 1.8 S/m is built by mixing polythene powder, TX151, and water. The recipe given in [22] is reproduced. Clingfilm is used to wrap the phantom to avoid evaporation and water penetration in the antennas, as seen in Figure 4a. The numerical phantom built in HFSS is identical to the one described above in order to assure agreement between simulations and measurements. The S-parameters of the antennas are measured using a 65-GHz Anritsu 37397C vector network analyzer (VNA). The same VNA is also used as a part of the radiation pattern measurement set-up in the University of Bristol's $8 \times 5 \times 4$ m pyramidal-cone anechoic chamber designed by Emerson and Cuming. The measurement set-up when the antennas were placed on the phantom can be seen in Figure 4b. The separation between the antennas and the body is varied from 0 mm to 10 mm with 5-mm increments using ECCOSTOCK PP.

4. Performance analysis

Figures 5 and 6 show the frequency characteristics of both prototypes. Comparing the simulations with measurements, a shift in the center frequency of the off-body antenna in the order of 50 MHz is observed. However, the measurements agree well with the simulations in terms of the relation between modes and how they change once the length of the feedline is altered. The gain patterns for each antenna for all the scenarios with different antenna body separations are plotted in Figure 7, where the trend of the changes for different scenarios or different antenna/body separations can be compared. The efficiency values are listed in Table 2. All the efficiency results are obtained at 2.5 GHz in order to maintain consistency between the simulations and measurements. These results are discussed in detail in Sections 4.1, 4.2, and 4.3.
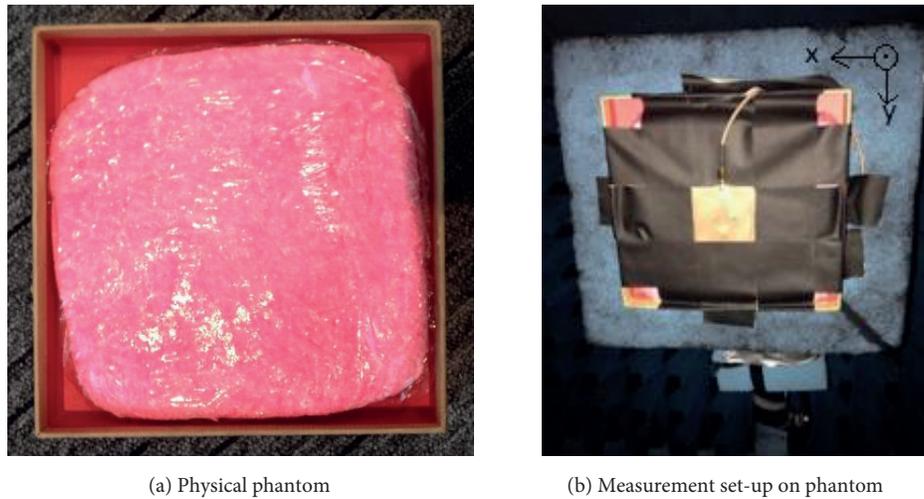
(a) Physical phantom

(b) Measurement set-up on phantom

Figure 4. The physical phantom used in the measurement (a) and the corresponding measurement set-up (b).
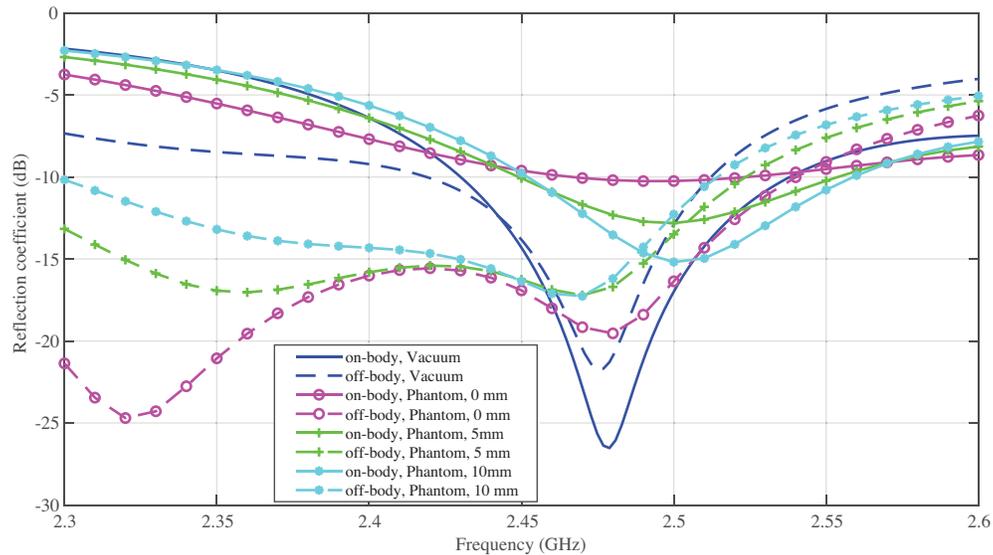

Figure 5. Simulated return loss of the prototypes for different scenarios for different antenna/body separations.

4.1. Frequency response

Figure 5 shows the frequency characteristics of the antennas according to the ANSYS HFSS simulations. A large drop in the magnitude of return loss is observed once the on-body antenna is located on the numerical chest phantom. This is due to the high permittivity value of the muscle rather than the conductivity, which was verified by the simulations. On the other hand, the off-body antenna's performance is less sensitive as compared to the on-body antenna. The off-body mode's ISM band coverage is maintained in all cases. Moving on to the measurements, Figure 6 demonstrates the antenna's response for different scenarios to the variation in the antenna-body separations. As predicted by the simulations, the on-body antenna's return loss is not as great as the off-body antenna's; however, both antennas are fairly stable against the changes in their near-field. The center frequency of the off-body antenna remains at 2.52 GHz for the phantom and Subject A, while it shifts to 2.51 GHz for Subject B. Note that Subject B has less fat in his body composition. For the on-body antenna,
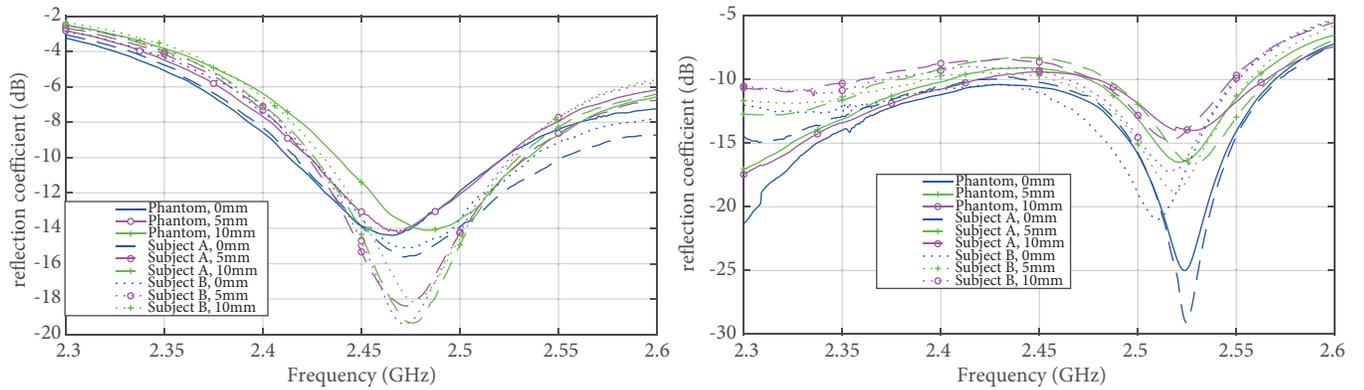
Figure 6. Measured return loss of the prototypes on a physical phantom and on 2 male subjects with antenna/body separations of 0 mm, 5 mm, and 10 mm: a) |S11| (dB) vs. Frequency (GHz) of the on-body antenna; b) |S11| (dB) vs. Frequency (GHz) of the off-body antenna.

Table 2. Radiation efficiency (5%).

Scenario	Measured efficiency	Simulated efficiency
Off-body in vacuum	NA	56
Off-body on RAM, 0 mm separation	41	NA
Off-body on RAM, 5 mm separation	41	NA
Off-body on RAM, 10 mm separation	42	NA
Off-body on phantom, 0 mm separation	34	41
Off-body on phantom, 5 mm separation	34	43
Off-body on phantom, 10 mm separation	36	45
On-body in vacuum	NA	76
On-body on RAM, 0 mm separation	45	NA
On-body on RAM, 5 mm separation	48	NA
On-body on RAM, 10 mm separation	49	NA
On-body on phantom, 0 mm separation	39	44
On-body on phantom, 5 mm separation	42	50
On-body on phantom, 10 mm separation	43	53

the center frequency remains at 2.47 most of the time, which shows that the on-body antenna is more immune to changes in body composition. In terms of the frequency response, the antenna satisfies the requirements of a BAN antenna and can be used near lossy environments. The return losses of both antennas for all scenarios are above 10 dB at 2.5 GHz. Therefore, 2.5 GHz is chosen as the frequency of measurement for the prototyped off-body and on-body antennas during the radiation pattern measurements.

4.2. Radiation pattern

Figures 7a–7p show the gain patterns of the on-body and off-body antennas in vacuum, on RAM, and on the previously described single-layer flat phantom mimicking the chest of an individual. In Figure 7a the on-body antenna generates an omnidirectional radiation pattern in its horizontal plane at 2.5 GHz. The complimentary
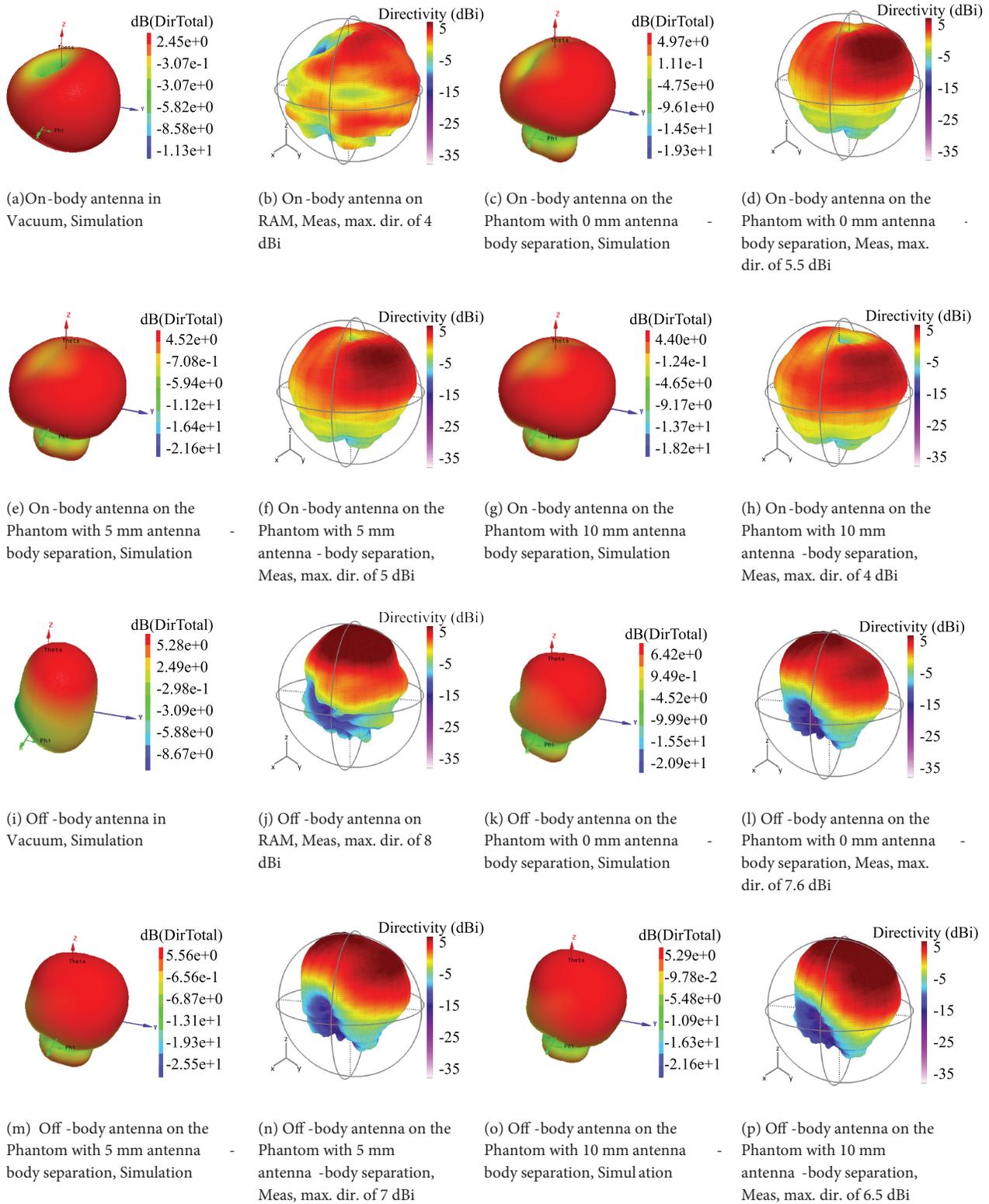
(a)On-body antenna in Vacuum, Simulation

(b) On-body antenna on RAM, Meas, max. dir. of 4 dBi

(c) On-body antenna on the Phantom with 0 mm antenna - body separation, Simulation

(d) On-body antenna on the Phantom with 0 mm antenna - body separation, Meas, max. dir. of 5.5 dBi

(e) On-body antenna on the Phantom with 5 mm antenna - body separation, Simulation

(f) On-body antenna on the Phantom with 5 mm antenna - body separation, Meas, max. dir. of 5 dBi

(g) On-body antenna on the Phantom with 10 mm antenna body separation, Simulation

(h) On-body antenna on the Phantom with 10 mm antenna -body separation, Meas, max. dir. of 4 dBi

(i) Off-body antenna in Vacuum, Simulation

(j) Off-body antenna on RAM, Meas, max. dir. of 8 dBi

(k) Off-body antenna on the Phantom with 0 mm antenna - body separation, Simulation

(l) Off-body antenna on the Phantom with 0 mm antenna - body separation, Meas, max. dir. of 7.6 dBi

(m) Off-body antenna on the Phantom with 5 mm antenna - body separation, Simulation

(n) Off-body antenna on the Phantom with 5 mm antenna -body separation, Meas, max. dir. of 7 dBi

(o) Off-body antenna on the Phantom with 10 mm antenna body separation, Simulation

(p) Off-body antenna on the Phantom with 10 mm antenna -body separation, Meas, max. dir. of 6.5 dBi

Figure 7. Simulated and measured 3D radiation patterns of the on-body and the off-body antennas at 2.5 GHz in vacuum (on RAM for measurements) and on the phantom with 0 mm, 5 mm, and 10 mm antenna phantom separations.

measurement is shown in Figure 7b. Although the antenna generates a null at $\theta = 0°$ as predicted, the pattern is distorted. This is due to the fact that the antenna is measured on a block of RAM backed with a metal rotating post carrying the antenna. Therefore, the antenna does not act in a way identical to how it acts in vacuum. When the on-body antenna is positioned on the phantom, the agreement between the simulations and the measurements get much better. Comparing Figures 7a and 7c, it can be observed that once the antenna is positioned on the body phantom, its radiation is shifted in the vertical direction and the energy will be emitted mostly in the positive half-space. This is favorable considering the specific absorption rate (SAR). Finally, Figures 7c–7h show that the null at $\theta = 0°$ is maintained in all cases.

In vacuum, the off-body antenna generates a directional pattern at 2.5 GHz and the measured half-power beam width is approximately $100°$; see Figures 7i and 7j. Comparing these figures, the agreement between the simulation in vacuum and the measurement on RAM is better compared to the on-body antenna case since the off-body antenna's radiation in the lower half-space is minimal. When the off-body antenna is located on the phantom, the pattern goes through slight changes as predicted by the simulations. However, its directional nature is maintained, making it suitable for off-body communications. In all measured results, the effect of the feed connector is visible, which is positioned along the negative x-axis of the radiation pattern. This distortion leads to a slight increase in the cross-polarization levels of the off-body antenna. When the off-body antenna and the on-body antenna are simulated and measured on the phantom with different separations from 0 mm to 10 mm with 5-mm increments, the radiation patterns remain directional and omnidirectional, respectively. Both antennas show little backward radiation, which restricts the absorption by the phantom. This is because the proposed antennas incorporate a full ground plane below their main radiator.

4.3. Efficiency

Radiation efficiency is one of the key performance metrics of a BAN antenna [23]. Dielectric and conductive losses determine the radiation efficiency and measuring these quantities is not straightforward. Here, the method of comparative testing described in [24] is followed. An antenna that is assumed to be highly efficient is compared to the antenna under test (AUT) through full three-dimensional radiation pattern measurements. A square patch antenna on air with a large ground plane is used as the reference antenna.

The comparison is represented by Eq. (1), where E, η_m, and η_Ω stand for the electric field level, the mismatch efficiency, and the conductor and dielectric losses, respectively.

$$\frac{\iint |\mathbf{E_{AUT}}|^2 \, \mathbf{dS}}{\iint |\mathbf{E_{REF}}|^2 \, \mathbf{dS}} = \frac{\eta_{mAUT} \eta_{AUT}}{\eta_{mREF} \eta_{REF}} \tag{1}$$

The antennas are located on a block of RAM as well as on the phantom, and the antenna/body separation is changed from 0 mm to 10 mm with 5-mm increments for each efficiency measurement. In order to achieve as much accuracy as possible the measurements are repeated three times and the results are averaged. Moreover, the environment is kept as constant as possible and the reference antenna measurements are repeated each time with AUT measurements. This method results in a characteristic 5% variation in the figures. Note that the cable losses are inherently cancelled since the same cables are used for the reference antenna and the AUTs. As seen in Table 2, the measured results are aligned with the simulated results although the measured values are always lower than the predicted values. The efficiency values do not change significantly for the off-body antenna when it is placed on the RAM and on the phantom with different spacings.

Therefore, the efficiency of the off-body antenna was found to be insensitive to the phantom, which was

the case for the radiation pattern analysis, as well. In contrast, the on-body antenna's efficiency improves by approximately 5% as the separation increases from 0 mm to 10 mm for both scenarios. These results agree with the previous radiation pattern analysis. The relatively higher improvement is because the on-body antenna has an omnidirectional pattern and less energy is absorbed by the phantom as the separation increases. Although the simulated radiation efficiencies shown in Table 2 are calculated at 2.5 GHz, additional efficiency values are calculated at 2.47 GHz, 2.48 GHz, and 2.55 GHz. The results show that both antennas can get 5%–10% higher radiation efficiency at other frequencies. Therefore, it can be estimated that the antennas can exhibit better efficiency performance after precise design. The performance analysis shows that the antenna is fairly immune to detuning. The frequency coverage is stable as the scenarios and the antenna/body separation change and the efficiency degradation is in the order of 5% as the antenna/body separation approaches 0 from 10 mm. It is capable of creating two distinct radiation patterns, which is going to improve the quality of the BAN links. Taking all these parameters into account, in a scenario where two on-body sensors located in the same horizontal plane and an off-body gateway located in the vertical direction to one of the on-body sensors are communicating using the proposed antenna, depending on the relative angle of one on-body sensor to the other, the improvement in the on-body link could potentially range between 18 dB and 5 dB compared to the case where the off-body modes are used to realize this link. On the other hand, the improvement in the off-body link between the off-body gateway and the on-body sensor located in the same vertical plane as the off-body gateway is going to be 11 dB compared to the case where the on-body modes are used to realize this link.

5. Conclusion

A novel on-body antenna that achieves radiation pattern diversity was presented in this paper. The antenna can generate two dissimilar modes, which can be activated or deactivated using a switching mechanism in order to proficiently support off-body and an on-body links. The switching was left out of the scope of this paper and the two modes were validated using two separate antennas. The performance of each mode was analyzed through HFSS simulations and measurements were taken at the University of Bristol. The analysis proved that the antenna is suitable for operating near the human body while maintaining its frequency characteristics and radiation performance even with minimal separation between the antenna and the skin. Moreover, the radiation efficiency of each mode is at an acceptable level. As a result, the average link quality and hence the overall efficiency of the system is expected to improve.

Acknowledgment

References

[1] Dumanli S, Gormus S, Craddock IJ. Energy efficient body area networking based on off-the-shelf wireless sensors. In: Proceedings of the 8th International Conference on Body Area Networks; 2013; Boston, MA, USA.

[2] Mellios E, Goulianos A, Dumanli S, Hilton GS, Piechocki RJ, Craddock IJ. Off-body channel measurements at 2.4 GHz and 868 MHz in an indoor environment. In: Proceedings of the 9th International Conference on Body Area Networks; 2014; London, UK.

[3] Hall PS, Hao Y. Antennas and propagation for body centric communications. In: Proceedings of the European Conference on Antennas and Propagation; 2006; Nice, France. pp. 1-7.

[4] Conway GA, Scanlon WG. Antennas for over-body-surface communication at 2.45 GHz. IEEE T Antenn Propag 2009; 57: 844-855.

[5] Locher I, Klemm M, Kirstein T, Troster G. Design and characterization of purely textile patch antennas. IEEE T Adv Packaging 2006; 29: 777-788.

[6] Sanz-Izquierdo B, Huang F, Batchelor JC. Covert dual-band wearable button antenna. Electron Lett 2006; 42:3-44.

[7] Ogawa K, Uwano T, Takahashi M. A shoulder-mounted planar antenna for mobile radio applications. IEEE T Veh Technol 2000; 49:1041-1044.

[8] Hall PS, Hao Y, Nechayev YI, Alomainy A, Constantinou CC, Parini C, Kamarudin MR, Salim TZ, Hee DTM, Dubrovka R et al. Antennas and propagation for on-body communication systems. IEEE Antenn Propag M 2007; 49: 41-58.

[9] Nechayev YI, Hall PS, Khan I, Constantinou CC. Wireless channels and antennas for body-area-networks. In: Seventh International Conference on Wireless On-demand Network Systems and Services; 2010; Kranjska Gora, Slovenia. pp. 137-144.

[10] Alves T, Poussot B, Laheurte JM. Analytical propagation modeling of BAN channels based on the creeping-wave theory. IEEE T Antenn Propag 2011; 59: 1269-1274.

[11] Raman S, Graham B, Crossan SM, Timmons N, Morrison J, Shameena VA, Pezholil M. Microstrip fed ground modified compact antenna with reconfigurable radiation pattern for BANs. In: Loughborough Antennas and Propagation Conference; 2012; Loughborough, UK. pp. 1-4.

[12] Masood R, Person C, Sauleau R. A dual-mode, dual-port pattern diversity antenna for 2.45-GHz WBAN. IEEE Antenn Wirel Pr 2017; 16: 1064-1067.

[13] Herscovici N, Christodoulou C, Rajo-Iglesias E, Quevedo-Teruel O, Sanchez-Fernandez M. Compact multimode patch antennas for MIMO applications [Wireless Corner]. IEEE Antenn Propag M 2008; 50: 197-205.

[14] Dumanli S. On-body antenna with reconfigurable radiation pattern. In: 2014 IEEE MTT-S International Microwave Workshop Series on RF and Wireless Technologies for Biomedical and Healthcare Applicationsl 2014; London, UK. pp. 1-3.

[15] Kikuzuki T, Andrenko AS, Hossain MGS, Ida I, Kasai K, Ohashi Y. A simple path loss model for body area network in the bed side monitoring applications. In: Asia-Pacific Microwave Conference Proceedings; December 2011; Melbourne, Australia. pp. 765-768.

[16] Gonzalez-Posadas V, Segovia-Vargas D, Rajo-Iglesias E, Vazquez-Roy JL, Martin-Pascual C. Approximate analysis of short circuited ring patch antenna working at TM01 mode. IEEE T Antenn Propag 2006; 54:1875-1879.

[17] Merce N, Tejedor P, Vassal'lo J. The TM01 mode of microstrip radiators and some of its applications. In: Ninth International Conference on Antennas and Propagation; 1995; Eindhoven, the Netherlands. pp. 33-36.

[18] Martin-Pascual C, Seoane I. On the generation and applications of the monopolar ("zeroth" like) mode in noncircular patches. In: 17th International Conference on Applied Electromagnetics and Communications; October 2003; Dubrovnik, Croatia. pp. 160-163.

[19] ANSYS. Inc. ANSYS HFSS. Canonsburg, PA, USA: ANSYS, Inc., 2016.

[20] Gabriel S, Lau RW, Gabriel C. The dielectric properties of biological tissues: III. Parametric models for the dielectric spectrum of tissues. Phys Med Biol 1996; 41: 2271-2293.

[21] Augustine R. Electromagnetic modelling of human tissues and its application on the interaction between antenna and human body in the BAN context. PhD, University of Paris-Est, Paris, France, 2009.

[22] Giddens H, Paul DL, Hilton GS, McGeehan JP. Numerical and experimental evaluation of phantoms for off-body wireless communications. In: Proceedings of the Loughborough Antennas & Propagation; Loughborough, UK. 2011. pp. 1415-2011.

[23] Paul D, Giddens H, Paterson M, Hilton G, McGeehan J. Impact of body and clothing on a wearable textile dual band antenna at digital television and wireless communications bands. IEEE T Antenn Propag 2013; 61: 2188-2194.

[24] Hilton GS, Hunt-Grubbe HWW. Simulation and practical analysis of a cavity-backed linear slot antenna for operation in the IEEE802.11a band. In: European Conformal Antenna Workshop; September 2007; Bristol, UK.